3D Solid Finite-Element Analysis of Cyclically Loaded RC Structures Allowing Embedded Reinforcement Slippage

G. C. Lykidis[1] and K. V. Spiliopoulos[2]

Abstract: It is a well established experimental fact that slippage of reinforcement may sometimes play an important role in the response of cyclically loaded reinforced concrete (RC) structures, especially in cases of beam-column subassemblages. In the past, analyses with 2D plane or 3D solid finite elements that assume a nonlinear bond-slip relationship to describe an arbitrary response of the interface have only been performed using elements connecting concrete nodes with discrete reinforcement nodes. This modeling exhibits restrictions in the bar topology, which can be removed only with embedded reinforcement formulations. In the present work, a 3D solid element, based on a simple smeared crack one-parameter model that describes concrete's triaxial stress-strain behavior is extended for cases of cyclically loaded RC structures, allowing embedded reinforcement slippage. This modeling is combined with an existing bond-slip mathematical description to give stable numerical results. The proposed procedure is applied successfully in a long anchorage rebar test, as well as two cases of bond critical exterior and interior column-beam joints, and numerical results compare well with existing experimental data.

DOI: 10.1061/(ASCE)0733-9445(2008)134:4(629)

CE Database subject headings: Concrete, reinforced; Slip; Finite elements method; Nonlinear analysis; Cyclic loads; Three-dimensional analysis; Beam columns; Joints.

Introduction

In order to evaluate the behavior of reinforced concrete (RC) structures, it is essential to be able to predict their response under any type and level of loading. To this end, the finite-element method of analysis may be used. For such an analysis to be realistic, one must take into account all aspects of the nonlinear behavior of RC including slippage of reinforcement, which can significantly affect the overall response, especially for high load levels, such as earthquake imposed ground acceleration (CEB 1996). Numerical modeling should take into account these effects in order to produce realistic predictions of strength, stiffness, and seismic energy dissipation capacity.

The main advantage of employing a computationally more expensive three-dimensional (3D) solid finite element for RC analysis is that it can take into account any triaxial stress state developed in almost all types of RC structures as well as modes of failure (e.g., brittle shear failure) that are not easily predicted by simpler methods. In such an analysis, there are three aspects that need to be considered: (a) modeling of concrete; (b) the material model to describe the behavior at the interface; and (c) modeling of reinforcement within the concrete mesh.

An extensive literature review regarding concrete modeling can be found elsewhere (ACI 1997). Smeared cracking appears to be the most popular method to analyze concrete structures by finite elements. According to this method, it is assumed that when a crack forms normal to the maximum principal tensile stress, stiffness is reduced perpendicularly to the crack plane (Rashid 1968). Several issues regarding mesh sensitivity due to strain localization (Bazant 1976) have been treated with the use of various methods (localization limiters), for example, the nonlocal continuum formulations of Bazant (1984).

In regard to (b), a thorough literature review up to 1996 can be found in CEB (1996). Eligehausen et al. (1983), after performing experiments on a large number of bars embedded in concrete for a small length, developed a model that can describe the local bond stress-slip relationship for arbitrary slip histories. In Filippou et al. (1983), a fourth order polynomial for unloading and reloading in the opposite direction is introduced. Lowes et al. (2004) present a bond-slip model that can take into account the status of the surrounding concrete (stress and damage) with the use of appropriate modification factors.

As far as (c) is concerned, the two major approaches are those with discrete or embedded reinforcement formulations, the most popular of the two being the former. Some of the more recent works using the first approach are by Coronelli and Mulas (2001) and Rabczuk et al. (2005) who present such methods for 2D analyses of structures under monotonic loading.

As far as embedded formulations are concerned, which are the ones adopted in the present work, Elwi and Hrudey (1989) develop an approach for simulating an embedded reinforcement bar inside a 2D concrete element. Slip along the bar is calculated using the slippage at additional degrees of freedom (d.o.f.) introduced at each bar node. Applications following this approach on RC structures under static monotonic loading were performed in

[1]Ph.D. Student, Institute of Structural Analysis and Aseismic Research, Dept. of Civil Engineering, National Technical Univ. of Athens, Zografou Campus, Athens 157-80, Greece. E-mail: glykid@mail.ntua.gr

[2]Associate Professor, Institute of Structural Analysis and Aseismic Research, Dept. of Civil Engineering, National Technical Univ. of Athens, Zografou Campus, Athens 157-80, Greece. E-mail: kvspilio@central.ntua.gr

Note. Associate Editor: Elisa D. Sotelino. Discussion open until September 1, 2008. Separate discussions must be submitted for individual papers. To extend the closing date by one month, a written request must be filed with the ASCE Managing Editor. The manuscript for this paper was submitted for review and possible publication on April 24, 2006; approved on October 18, 2007. This paper is part of the ***Journal of Structural Engineering***, Vol. 134, No. 4, April 1, 2008. ©ASCE, ISSN 0733-9445/2008/4-629–638/$25.00.

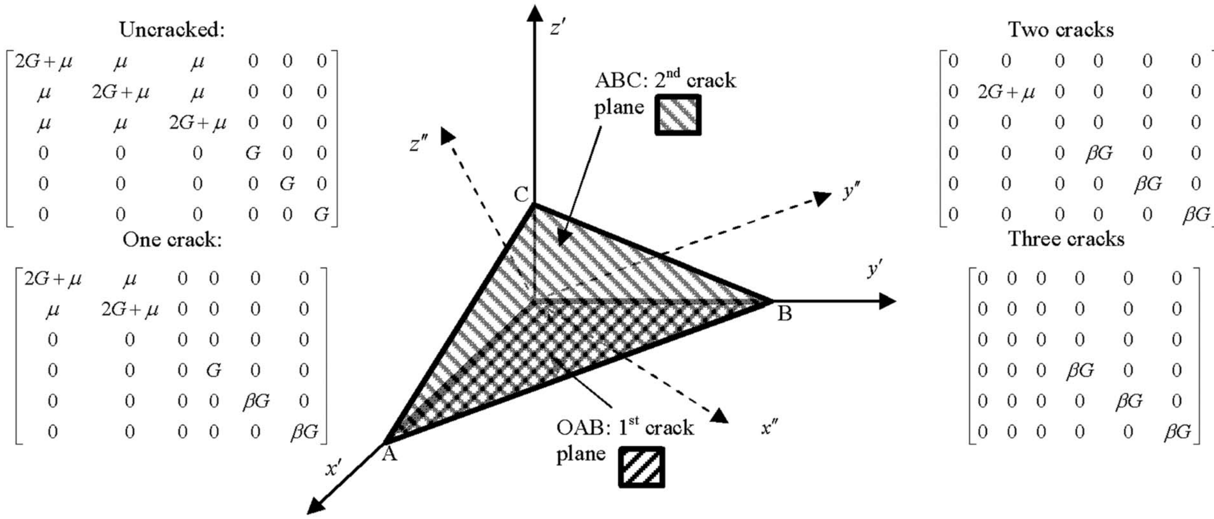

Fig. 1. Modification of concrete material matrix $\mathbf{D}_c$ according to the smeared crack approach: uncracked material, loss of stiffness along z' axis due to first crack, additional loss of stiffness along x'' axis due to second crack, loss of stiffness along all axes due to third crack

3D by Barzegar and Maddipudi (1997) with a cubic relation between bond stress and slip and in 2D by Kwak and Filippou (1997) with a trilinear one. Hartl (2002) develops two distinct formulations: An embedded bar allowing slip and an alternative embedded bar formulation named as "supplementary interface model," which considers the two materials as two substructures. He only implements the second method in a finite-element code.

As far as cyclic actions are concerned, Lowes (1999) and Fleury et al. (1999) perform 2D analyses of joints using a bond element of zero width to connect concrete and steel nodes. A fiber RC element that allows for bar slipping has been presented in Monti and Spacone (2000), Limkatanyu and Spacone (2003), and Ayoub (2006) to analyze RC columns. Girard and Bastien (2002) present an application with 20-node hexahedral finite elements with discrete reinforcement bars to analyze a RC column. The interface is described with a bilinear model with kinematic hardening.

It is clear that a discrete bar modeling instead of an embedded one, arbitrarily within the concrete finite-element mesh, exhibits too many restrictions for the analyst. Nevertheless, although the formulations for partially bonded embedded reinforcement have appeared since Elwi and Hrudey (1989), no analyses of RC structures under cyclic loading using 3D solid finite elements with embedded bars are known to the authors to have been presented in the literature up to date.

In the present work, a simple smeared crack material model for 3D solid concrete elements (Kotsovos and Pavlovic 1995) that requires only the uniaxial compressive concrete strength f_c as input, with a crack strategy employed by Spiliopoulos and Lykidis (2006) that proved to give stable numerical results assuming full bond conditions, is adopted. This crack strategy is herein combined with the embedded reinforcement formulations with slip (Barzegar and Maddipudi 1997) and the bond-slip mathematical description of Eligehausen et al. (1983). Despite all the types of high nonlinearity of the problem at hand, the procedure proves to be numerically stable. It is then applied to a reinforcing bar embedded in concrete and two RC joints, all subjected to cyclic loading. Results show that this combination proves to give much more realistic predictions compared to those obtained by analyses that do not allow slippage of reinforcement.

Material Modeling

Concrete

The 3D constitutive behavior of concrete is divided in two separate states: (I) before macrocracking and (II) after macrocracking.

For state I, where concrete exhibits a small degree of nonlinearity, it is assumed that the behavior is essentially isotropic and that under pure hydrostatic stress, concrete only develops hydrostatic strains, whereas under deviatoric stress, concrete develops both hydrostatic and deviatoric strains. The constitutive relations depend only on the concrete uniaxial compressive strength f_c (Kotsovos and Pavlovic 1995). Unloading and subsequent reloading follow the initial stiffness slope using a criteria that compares the current deviatoric stress with the highest deviatoric stress previously experienced by the material.

The hydrostatic and deviatoric stresses serve also as a means to describe concrete failure resulting in macrocracking (state II) represented in the three-dimensional principal stress space by an open and convex failure surface, also depending on the parameter f_c as given by Kotsovos and Pavlovic 1995.

A smeared crack model within the framework of the finite-element method is used to simulate the effect of cracking in the structure. At a Gauss point (GP), when the failure surface is exceeded for the first time, a crack perpendicular to the maximum tensile stress is formed resulting in a subsequent modification of the stiffness, indicating no resistance perpendicular to the crack and small shear resistance on its plane modeled with the use of a shear retention factor β. Should a second crack form at the same GP, then further modification will take place, leaving resistance only along the line of intersection of the two planes. In case a third crack forms, then a complete loss of the load carrying capacity occurs. All the various modifications of the material matrix D_c, which relates the incremental stresses with strains, are shown in Fig. 1, where G and μ are the tangential Lamé's constants that may be determined for the current stress state using once again f_c only. A more extensive description may be found in Kotsovos and Pavlovic (1995) as well as Spiliopoulos and Lykidis (2006).

The fully brittle nature of the above material description raises issues regarding mesh inobjectivity due to strain localization

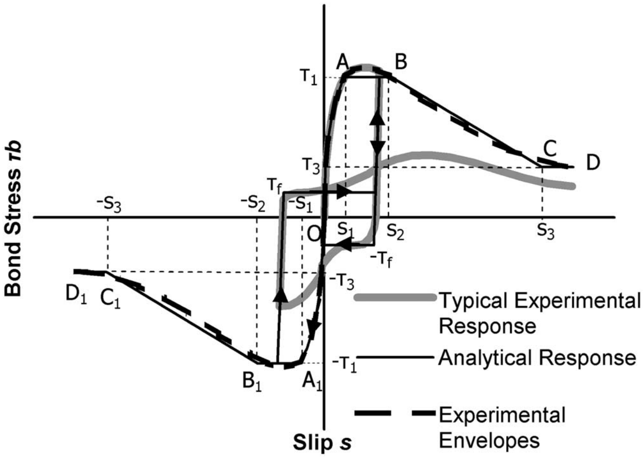

Fig. 2. Typical bond stress-slip relationship of a reinforcement bar embedded in concrete, experimental curves and corresponding analytical prediction with the assumed model

(Bazant 1976). All successful analyses in terms of realistic predictions presented to date with the use of this model have used a coarse mesh with elements having a size from 5 to 20 cm. Limiting the element size to this range seems to provide results that match well with experimental evidence.

Steel

The Menegotto Pinto (1973) model is adopted. This model has proved to give realistic predictions for steel bar behavior, since it accommodates the Bauschinger effect, observed under large load reversals.

Interface

The numerical modeling of the interface behavior is performed using the mathematical description of Eligehausen et al. (1983). Typical experimental and analytical bond stress $(\tau_b)-$slip (s) relationships are presented in Fig. 2. The positive monotonic envelope OABCD (or the negative $OA_1B_1C_1D_1$), consisted of an ascending branch (OA), a constant stress part (AB), a descending branch (BC), and a constant friction branch (CD), is the basis on which the behavior is determined for any given slip history. The envelope can be fully described by the values s_1, s_2, s_3, τ_1, and τ_3 and no reductions to them to account for damage are considered in this work. For this reason, there could be an overestimation of the predicted strength, for example as shown in Fig. 2 where the typical experimental response gives a smaller strength after one cycle.

In Eligehausen et al. (1983), it is proposed that the first branch (OA) is described by Eq. (1)

$$\tau_b = \tau_1 \left(\frac{s}{s_1}\right)^{\alpha} \tag{1}$$

This function of bond stress has an infinite initial slope and therefore no explicit way to form the initial stiffness matrix exists. For this reason, it is more convenient to use a parabola according to Eq. (2)

$$\tau_b = \tau_1 \left(2 - \frac{s}{s_1}\right)\frac{s}{s_1} \tag{2}$$

Although this modification has never been mentioned in the literature, it has been used in the Fedeas Library (2006). By choosing the parabola [Eq. (2)] instead of the exponential function [Eq. (1)], the nonlinearities are underestimated in the first branch, something that is a small penalty if predictions at large slip values are sought.

The rest of the branches that comprise the monotonic envelope are linear relations between bond stress and slip. Reverse loading is performed initially using the elastic tangent stiffness up to the point where a bond stress equal to the value of friction stress τ_f of the opposite sign is reached. A constant friction branch τ_f is then followed until it meets the monotonic envelope of the opposite sign. A complete load cycle can be seen in Fig. 2.

In this work, the current friction bond stress τ_f is evaluated according to the expression

$$\tau_f = \tau_3 \cdot \min\left(1.00, \frac{s^+_{\max} - s^-_{\min}}{s^+_2 - s^-_2}\right) \tag{3}$$

where $s^+_{\max}$, $s^-_{\min}$=maximum positive and minimum negative slips, respectively, exhibited up to the current state, and s^+_2, s^-_2=corresponding s_2 values for the positive and negative monotonic envelopes, respectively.

Reinforcement Modeling

Rebar Meshing

In the present approach, 27-node solid finite elements with $3\times3\times3$ GP are used for concrete, whereas three-node embedded truss elements with three GP model steel bars.

In RC modeling with 3D solid finite elements, it is very convenient for the analyst to be able to model bars using their end coordinates, without explicitly stating the discretization of the bar into the concrete finite-element mesh. Barzegar and Maddipudi (1994), continuing the work of Elwi and Hrudey (1989), have developed a method to perform this task. This approach has been followed in Spiliopoulos and Lykidis (2006) as well as in the present work.

Embedded Reinforcement Allowing Slip Formulations

Different approaches regarding the development of the relevant formulations have been presented in the literature (Elwi and Hrudey 1989; Barzegar and Maddipudi 1997; Hartl 2002). Following an analogous approach, in this section, the equations are derived in a general form for parent concrete brick elements and embedded reinforcement consisting of truss elements. An additional d.o.f. representing slip is assumed for each of the truss nodes.

A steel bar slips through concrete by a relative displacement s, which is added to the parent concrete element's displacements u_c in order to determine the actual displacement field u_r, which deforms a bar having direction cosines l_1, m_1, n_1

$$u_r = u_c + s \text{ with } u_c = \{l_1 \quad m_1 \quad n_1\} \cdot \begin{Bmatrix} u_{c,x} \\ u_{c,y} \\ u_{c,z} \end{Bmatrix} \tag{4}$$

Strain at any given point of the bar can be expressed as

$$\varepsilon_r = \frac{du_r}{dl} = \frac{du_c}{dl} + \frac{ds}{dl} = \varepsilon_{c,r} + \frac{ds}{dl} \tag{5}$$

Assuming that $\mathbf{d}$ are the parent element's nodal displacements, axial strain $\varepsilon_{c,r}$ at any given point of the bar can be calculated from global concrete strains ε_c

$$\varepsilon_{c,r} = \mathbf{T}^* \cdot \boldsymbol{\varepsilon}_c = \mathbf{T}^* \cdot \mathbf{B}_c \cdot \mathbf{d}$$

with

$$\mathbf{T}^* = \{l_1^2 \quad m_1^2 \quad n_1^2 \quad l_1 m_1 \quad m_1 n_1 \quad l_1 n_1\} \tag{6}$$

where $\mathbf{B}_c$ are the shape function derivatives for the parent concrete element.

Assuming that the slip field along the bar is expressed through the truss element's shape functions $\mathbf{N}_r$ and the slip at the truss element's nodes $\mathbf{u}_{\text{slip}}$, the slip at any point may be expressed in the form of Eq. (7)

$$s = \mathbf{N}_r \cdot \mathbf{u}_{\text{slip}} \Rightarrow \tag{7}$$

$$\frac{ds}{dl} = \frac{d\mathbf{N}_r}{dl} \cdot \mathbf{u}_{\text{slip}} = \mathbf{B}_r \cdot \mathbf{u}_{\text{slip}} \tag{8}$$

It should be noted at this point that in reinforced concrete when a crack forms, the local slip distribution of an intersecting reinforcement bar could certainly not be predicted accurately by the smeared crack approach in which cracks are assumed smeared over the volume sampled by a GP. For this reason, the use of the shape functions of Eq. (7) for a cracked finite element might not be very accurate for the estimation of the bond state locally, but it could give meaningful results for the overall rebar behavior in the corresponding structural members.

Eq. (5) can be written as

$$\varepsilon_r = [\mathbf{T}^*\mathbf{B}_c \quad \mathbf{B}_r]\begin{Bmatrix}\mathbf{d}\\ \mathbf{u}_{\text{slip}}\end{Bmatrix} = \mathbf{B}^* \cdot \mathbf{d}^* \tag{9}$$

Having found the solution at step t equilibrating an external force vector $\mathbf{R}_t$ applied on all concrete nodes, and/or any external loading $\mathbf{P}_t$ applied on the interface nodes (e.g., prestressing), the incremental form of the virtual work principle may be used to obtain the solution at step $t+\Delta t$

$$\int_{V_r} \delta\Delta\varepsilon_r \cdot (\sigma_r + \Delta\sigma_r) dV_r + \int_L \delta\Delta s \cdot (\tau_b + \Delta\tau_b) dL + \int_{V_c} \delta\Delta\boldsymbol{\varepsilon}_c^T \cdot (\boldsymbol{\sigma}_c + \Delta\boldsymbol{\sigma}_c) dV_c = \delta\Delta\mathbf{d}^T \cdot \mathbf{R}_{t+\Delta t} + \delta\Delta\mathbf{u}_{\text{slip}}^T \cdot \mathbf{P}_{t+\Delta t} \tag{10}$$

with V_r, V_c=steel and concrete volumes, respectively, and L=external surface area of the bar.

The increments of stresses may be found from the increments of the corresponding strains and slip displacements using the tangent material properties

$$\Delta\boldsymbol{\sigma}_c = \mathbf{D}_c \cdot \Delta\boldsymbol{\varepsilon}_c \quad \Delta\sigma_r = E_r \cdot \Delta\varepsilon_r \quad \Delta\tau_b = k \cdot \Delta s \tag{11}$$

with O_r the bar section perimeter, A_r the bar section area and l its length, the expressions for dV_r and dL are

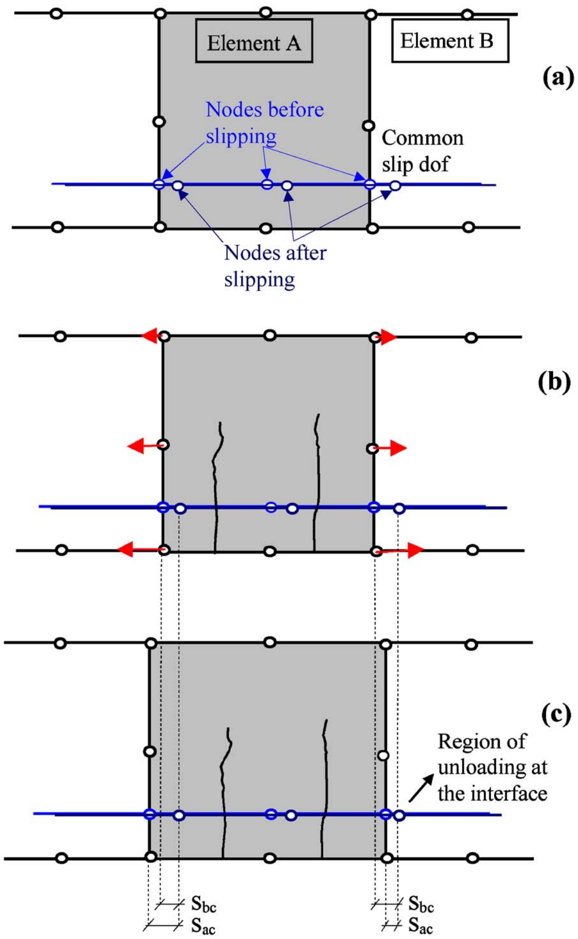

Fig. 3. Effect of cracking on the interface. s_{bc}=slippage before cracking, s_{ac}=slippage after cracking. (a) Slipped bar inside element before cracking; (b) residual forces caused by cracking; and (c) deformation of element due to residual forces and effect on bar slipping.

$$dV_r = A_r \cdot dl \quad dL = O_r \cdot dl \tag{12}$$

Substituting the above as well as Eq. (9) in Eq. (10), we get

$$\begin{aligned} &\int_l [\delta(\mathbf{B}^*\Delta\mathbf{d}^*)^T \cdot E_r \cdot (\mathbf{B}^*\Delta\mathbf{d}^*) \cdot A_r \\ &\quad + \delta(\mathbf{N}_r\Delta\mathbf{u}_{\text{slip}})^T \cdot k \cdot (\mathbf{N}_r\Delta\mathbf{u}_{\text{slip}}) \cdot O_r] dl \\ &\quad + \int_l [\delta(\mathbf{B}^*\Delta\mathbf{d}^*)^T \cdot \sigma_r \cdot A_r + \delta(\mathbf{N}_r\Delta\mathbf{u}_{\text{slip}})^T \cdot \tau_b \cdot O_r] dl \\ &\quad + \int_{V_c} \delta(\mathbf{B}_c \cdot \Delta\mathbf{d})^T [\boldsymbol{\sigma}_c + \mathbf{D}_c \cdot (\mathbf{B}_c \cdot \Delta\mathbf{d})] dV_c \\ &= \delta\Delta\mathbf{d}^T \cdot \mathbf{R}_{t+\Delta t} + \delta\Delta\mathbf{u}_{\text{slip}}^T \cdot \mathbf{P}_{t+\Delta t} \end{aligned} \tag{13}$$

Using Eq. (9) for $\mathbf{B}^*$, grouping similar terms and taking into account that this equation holds for any virtual displacement vector $\begin{Bmatrix}\delta\Delta\mathbf{d}\\ \delta\Delta\mathbf{u}_{\text{slip}}\end{Bmatrix}$, Eq. (13) can be finally written as

$$\left\{\begin{bmatrix} \mathbf{K}_{cc} + \mathbf{K}_{rr,c} & \mathbf{K}_{cr} \\ \mathbf{K}_{rc} & \mathbf{K}_{rr} + \mathbf{K}_{bb} \end{bmatrix} \cdot \begin{Bmatrix}\Delta\mathbf{d}\\ \Delta\mathbf{u}_{\text{slip}}\end{Bmatrix} + \begin{Bmatrix}\mathbf{Q}_{c,r}\\ \mathbf{Q}_b\end{Bmatrix}\right\} = \begin{Bmatrix}\mathbf{R}_{t+\Delta t}\\ \mathbf{P}_{t+\Delta t}\end{Bmatrix} \tag{14}$$

with

$$\mathbf{K}_{cc} = \int_{V_c} \mathbf{B}_c^T \cdot \mathbf{D}_c \cdot \mathbf{B}_c dV_c$$

$$\mathbf{K}_{rr,c} = \int_l \mathbf{B}_c^T \mathbf{T}^{*T} E_r A_r \mathbf{T}^* \mathbf{B}_c dl$$

$$\mathbf{K}_{cr} = \mathbf{K}_{rc}^T = \int_l \mathbf{B}_c^T \mathbf{T}^{*T} E_r A_r \mathbf{B}_r dl \tag{15}$$

$$\mathbf{K}_{rr} = \int_l \mathbf{B}_r^T E_r A_r \mathbf{B}_r dl \quad \mathbf{K}_{bb} = \int_l \mathbf{N}_r^T k O_r \mathbf{N}_r dl \tag{16}$$

$$\mathbf{Q}_{c,r} = \int_{V_c} \mathbf{B}_c^T \cdot \boldsymbol{\sigma}_c dV_c + \int_l \mathbf{B}_c^T \mathbf{T}^{*T} \sigma_r A_r dl$$

$$\mathbf{Q}_b = \int_l \mathbf{B}_r^T \sigma_r A_r dl + \int_l \mathbf{N}_r^T \tau_b O_r dl \tag{17}$$

For the general case of multiple bars nrs inside the concrete element, Eq. (14) takes the form

$$\begin{bmatrix} \mathbf{K}_{cc} + \sum_{i=1}^{nrs} \mathbf{K}_{rr,c,i} & \mathbf{K}_{cr,1} & \mathbf{K}_{cr,2} & \dots & \mathbf{K}_{cr,i} & \dots & \mathbf{K}_{cr,nrs} \\ \mathbf{K}_{rc,1} & \mathbf{K}_{rr,1} + \mathbf{K}_{bb,1} & \mathbf{0} & \dots & \mathbf{0} & \dots & \mathbf{0} \\ \mathbf{K}_{rc,2} & \mathbf{0} & \mathbf{K}_{rr,2} + \mathbf{K}_{bb,2} & \dots & \mathbf{0} & \dots & \mathbf{0} \\ \dots & \dots & \dots & \dots & \dots & \dots & \dots \\ \mathbf{K}_{rc,i} & \mathbf{0} & \mathbf{0} & \dots & \mathbf{K}_{rr,i} + \mathbf{K}_{bb,i} & \dots & \mathbf{0} \\ \dots & \dots & \dots & \dots & \dots & \dots & \dots \\ \mathbf{K}_{rc,nrs} & \mathbf{0} & \mathbf{0} & \dots & \mathbf{0} & \dots & \mathbf{K}_{rr,nrs} + \mathbf{K}_{bb,nrs} \end{bmatrix} \cdot \begin{Bmatrix} \Delta \mathbf{d} \\ \Delta \mathbf{u}_{\text{slip}} \end{Bmatrix} = \begin{Bmatrix} \mathbf{R}_{t+\Delta t} - \mathbf{Q}_{c,r} \\ \mathbf{P}_{t+\Delta t} - \mathbf{Q}_b \end{Bmatrix} \tag{18}$$

where now $\Delta \mathbf{u}_{\text{slip}}$ is a column vector that includes the slip displacements for all the embedded bars in the concrete element. These additional slip d.o.f. are common at the interface of two adjacent concrete elements [e.g., rebar passing Elements A and B at Fig. 3(a)]. For this reason they need to be present in the global structure stiffness matrix as separate d.o.f. and they cannot be condensed after the formation of the local element stiffness matrix.

If full bond is assumed, Eq. (18) becomes

$$\left[\mathbf{K}_{cc} + \sum_{i=1}^{nrs} \mathbf{K}_{rr,c,i} \right] \cdot \Delta \mathbf{d} = \mathbf{R}_{t+\Delta t} - \mathbf{Q}_{c,r} \tag{19}$$

If a concrete element does not contain any rebars, Eq. (18) becomes

$$[\mathbf{K}_{cc}] \cdot \Delta \mathbf{d} = \mathbf{R}_{t+\Delta t} - \mathbf{Q}_{c,r} \tag{20}$$

All three kinds of elements corresponding to Eqs. (18)–(20), should they exist in the structural model, can be readily used for the assembly of the global structure stiffness matrix using the connectivity of the concrete parent element and rebar nodes.

Implementation of the Numerical Procedure

This work has been based on the finite-element code developed in Spiliopoulos and Lykidis (2006). Large scale modifications were performed in the static analyses procedures in order to account for slippage of the embedded bars. An additional preprocessing procedure apart from the ones already described for the rebar meshing was needed to decide the position and correspondence of the additional d.o.f. along the reinforcement mesh. Each actual bar is followed from its beginning to its end, assigning the new d.o.f. of $\mathbf{u}_{\text{slip}}$ [Eq. (18)] for every node formed. The large number of zeros that inevitably exist in the global stiffness matrix due to the remote location of the slippage d.o.f., imposed the use of a sparse storage and handling scheme instead of the skyline algorithm (Bathe 1996) that was used in the previous code.

A direct displacement control (Jirasek and Bazant 2002), in the context of a full Newton-Raphson iterative procedure, is used to obtain the response of the examples presented herein. According to this procedure, initially all matrices and vectors are partitioned so that the d.o.f. are separated as "free" and "prescribed" ones. The "prescribed" d.o.f. include all supports as well as the nodes on which an imposed displacement is applied, whereas "free" d.o.f. are all the rest. In the first iteration of an incremental step, the entire increment of the displacements on the "prescribed" d.o.f. is applied. In all subsequent iterations, the incremental displacements on these d.o.f. are equaled to zero. Both the norms of the incremental displacements and reaction forces are compared for checking convergence of the iterative procedure.

In the present formulation, there are three sources of nonlinearities, i.e., concrete, steel, and interface. Possible opening, closure, and reopening of cracks in concrete may create residual stresses, which are integrated to equivalent nodal forces in the first term of the expression of $\mathbf{Q}_{\text{c,r}}$ [Eqs. (17)] using a strategy named the unified total crack approach (UTCA) (Spiliopoulos and Lykidis 2006). For the steel bars, residual stresses are determined from the increments of strains, and equivalent nodal forces are evaluated according to the second term of $\mathbf{Q}_{\text{c,r}}$ and the first term of $\mathbf{Q}_{\text{b}}$ [Eqs. (17)]. The residual bond stresses resulting from the slip increments are integrated in the expression for $\mathbf{Q}_{\text{b}}$ to give the residual bond forces, which need to be applied on the interface d.o.f. in the next iteration.

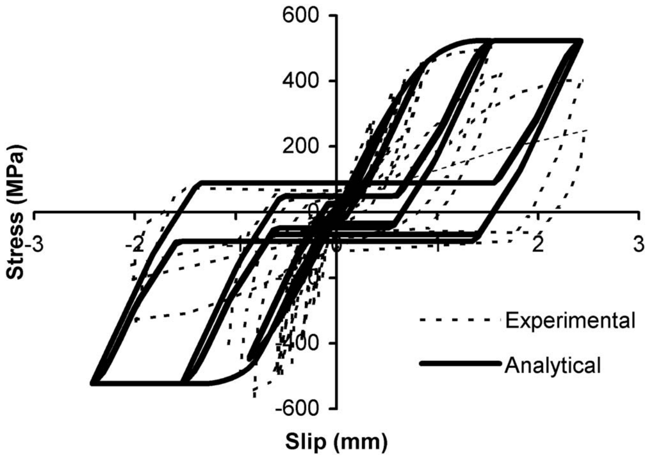

Fig. 4. Comparison of experimental and analytical stress-slip curves for the long anchorage tests of Viwathanatepa et al. (1979)

The various aspects of nonlinearity, especially for the case where nonlinear slippage is taken into account, result in a difficulty for the algorithm to converge. Even for monotonic loading, cracking may cause unloading in certain regions of the interface. For example, in Fig. 3(a) a bar embedded in a concrete finite element is assumed to have previously slipped after cracking has formed in the lower regions. This results in residual forces [Fig. 3(b)] that tend to deform the element in such a way that slippage on its left face tends to be increased ($s_{ac} > s_{bc}$) whereas on the right it tends to be reduced ($s_{ac} < s_{bc}$) [Fig. 3(c)]. Focusing on the right face of the concrete element, if the residual forces are large enough to cause a negative slip increment, which results in less total slip compared to the one at the previously converged step, unloading occurs at the interface and, therefore, new residual bond forces need to be introduced to the structure in the next iteration.

Applications

Although the examples presented could be analyzed with 2D plane elements, modeling of reinforced concrete structures with 3D solid elements and embedded reinforcement has the advantage of being straightforward, since all bars are positioned at their exact location (including stirrups). Any form of confinement is then automatically taken into account in the local concrete behavior without any explicit beforehand modification.

The original calibration tests on bars embedded in concrete for a small length (equal to five times the bar diameter) of Eligehausen et al. (1983) were reproduced according to the above procedure by Lykidis and Spiliopoulos (2006). In the sequel, applications on a long anchorage push-pull test and two bond critical beam-column joints under cyclic actions are presented.

Although different properties for bond slip along a bar may be used, in order to preserve the simplicity that the concrete model exhibits (since f_c is required as concrete's only material parameter), unique values for the envelope, both in tension and compression, are chosen. On the other hand, the use of a coarse mesh dictated by the nature of the concrete model, makes choosing more sophisticated varying bond properties along different parts of the bar meaningless.

Long Anchorage Specimen

A broad experimental investigation of the bond-slip behavior in long anchored reinforcing bars was performed in Viwathanatepa et al. (1979). Specimen 14, consisting of a $d_b = 25.4$ mm diameter bar embedded for a length equal to $25d_b$ in concrete, was experimentally tested under simultaneous cyclic push and pull at the two rebar ends. The loading history was reproduced numerically by fixing the two concrete faces at the two bar ends and by applying equal displacement at the corresponding slip d.o.f.

One 3D solid finite element was used for concrete with an embedded rebar having the following bond-slip properties: $s_1 = 0.75$ mm, $s_2 = 3.00$ mm, $s_3 = 10.50$ mm, $\tau_1 = 13.50$ MPa, $\tau_3 = 3.50$ MPa. These values match well with the ones previously used for the analysis of this experiment (Ciampi et al. 1982, Monti et al. 1997, Ayoub and Filippou 1999).

Despite the fact that only one element is used, the results show a very good prediction for slip values up to ±1 mm (Fig. 4). For larger values, it can be seen that an overestimation of the ultimate strength is predicted, which can be accredited to the assumption that no damage is considered in the bond-slip model.

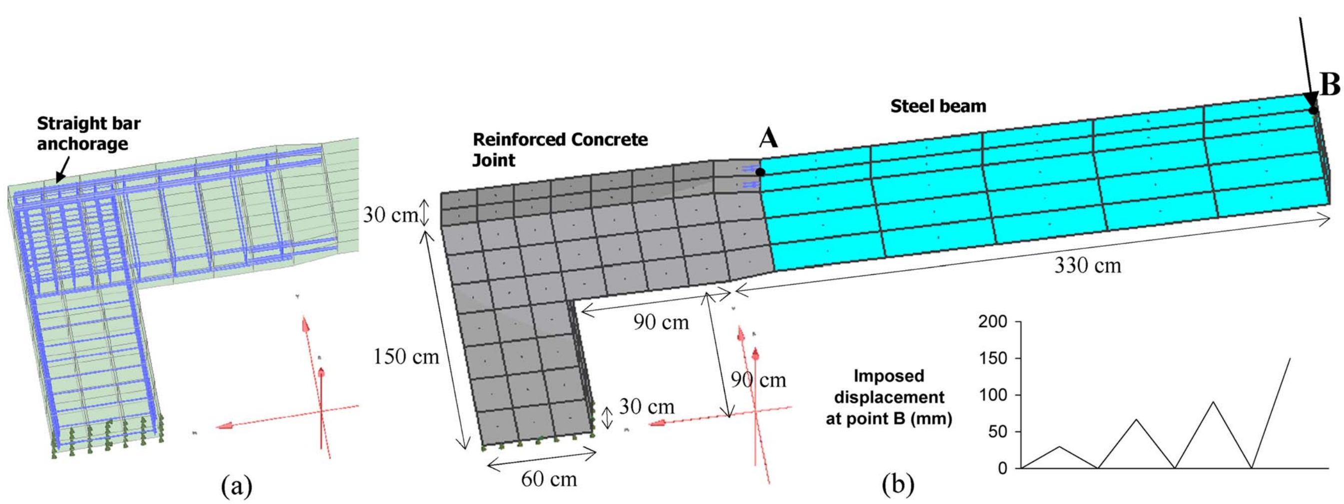

Fig. 5. (a) Embedded reinforcement mesh; (b) concrete and structural steel finite element mesh and applied displacement history

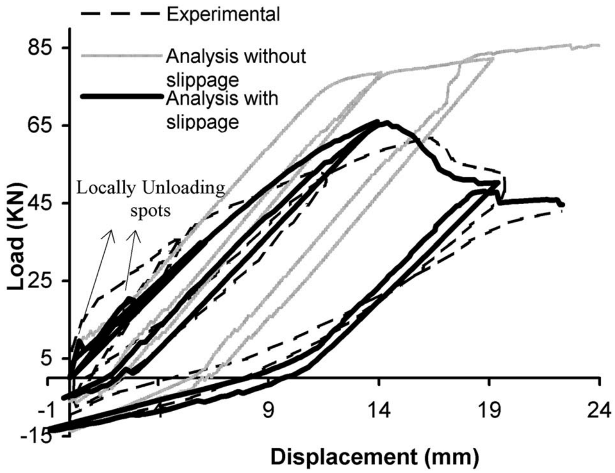

Fig. 6. Comparison of analytical predictions versus experimental measurement. Displacement is measured at the joint connection with the steel member [point A in Fig. 5(b)].

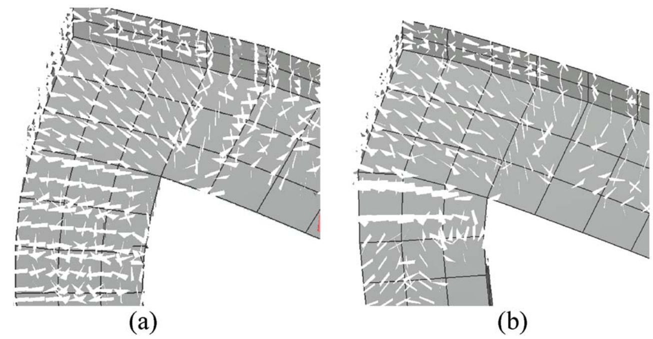

Fig. 7. Prediction of crack pattern analysis: (a) without slippage; (b) with slippage

Corner Beam Column Joint

A RC joint (Fig. 5) for which experimental data exist (Luiki 1999), was analyzed by Hartl (2002) and Lykidis and Spiliopoulos (2006) for monotonic loading. In the test, a cyclic loading was applied on the joint with the use of a steel beam girder. The longitudinal bars ending at the joint were designed with a straight anchorage [Fig. 5(a)] so that the failure mode would be due to slippage of reinforcement.

The joint is modeled and analyzed under imposed displacements at point B so that a bending moment and shear force are applied at the right section of the joint (point A). The experimental cyclic loading history [shown in Fig. 5(b)] is used in the analysis. The analytical prediction at point A confirms what was also observed in the experiment: A total displacement up to the value of 22.30 mm for point A is reached, with intermediate unloading down to zero and reloading up to the values of 5.00 mm, 14.40 mm, and 19.20 mm.

Seventy-two solid 27-node elements of a size of about $20 \times 20 \times 15$ cm are used for the reinforced concrete part of the specimen. The elements that model the steel beam are of the same type, but they are considered to be elastic with relatively large stiffness.

The following assumptions regarding material behavior were made: Concrete uniaxial compressive strength $f_c = 35$ MPa, steel initial elastic modulus $E_s = 206$ GPa, steel yield stress $f_y = 440$ and 550 MPa for the two different groups of reinforcing bars.

The bond-slip envelope $s_1 = 0.60$ mm, $s_2 = 0.80$ mm, $s_3 = 4$ mm, $\tau_1 = 3$ MPa, $\tau_3 = 1.5$ MPa was chosen to describe the interface along all bars either in tension or compression without classifying them as having poor or good bond conditions. These values are a compromise between the values suggested by CEB-FIP (1993) and Eurocode 2 for all these cases and the possible reduction due to damage between cycles.

Two kinds of analyses were performed, first assuming full bond and second assuming slipping on longitudinal bars but not along the stirrups. Results are given in Fig. 6, where it can be seen that the rigid bond analysis overestimates the overall strength of the joint, whereas the second analysis allowing slip gives much more realistic predictions. As far as stiffness is concerned, it can be seen that although at the beginning (for displacements less than 1 mm), the predicted matches the observed one, for slightly larger values initial cracking in the numerical model unrealistically shifts the load displacement curve to the right, meanwhile retaining large stiffness for a certain range. This could be due to the limitations of the concrete model, for which a complete and sudden loss of stress is assumed when a crack opens (Kotsovos and Pavlovic 1995). Nevertheless, subsequent global response over the whole sequence of the cycles is well predicted. The unloading spots near the origin captured by the direct displacement controlled analysis are due to the initial cracking.

The predicted cracking pattern, as well as the deformed reinforcement mesh during the last converged steps, are presented in Figs. 7 and 8. In the prediction of the analysis in which rebar slip was allowed, a slip mechanism inside the joint is revealed [Fig. 8(b)] together with thick cracks in the area below the joint [Fig. 7(b)]. These characteristics were also observed experimentally by Luiki (1999). As seen in Figs. 7(a) and 8(a), this behavior could not have been predicted by the full bond analysis.

Additionally, in Fig. 9, the bond stress magnitude distributions along the vertical exterior reinforcement bars are presented for four points (A to D) on the load history path. It can be seen that

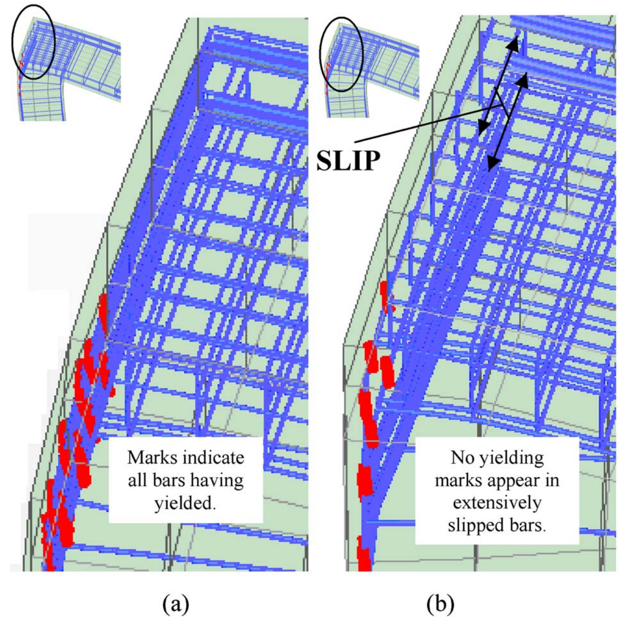

Fig. 8. Inside view of reinforcement at the corner regions: (a) analysis without slippage; (b) analysis with slippage

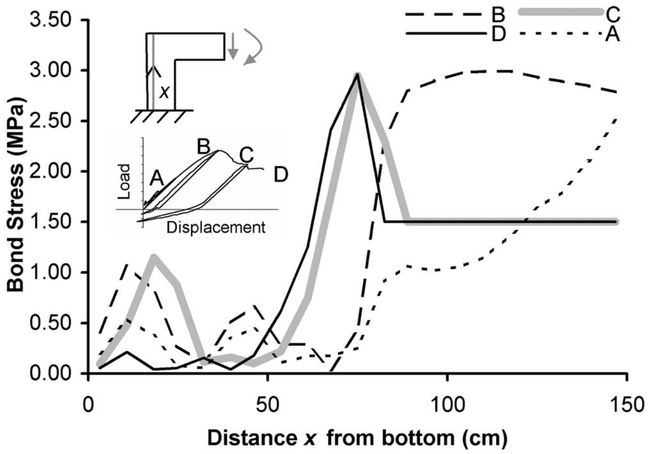

Fig. 9. Bond stress distribution along exterior vertical rebar

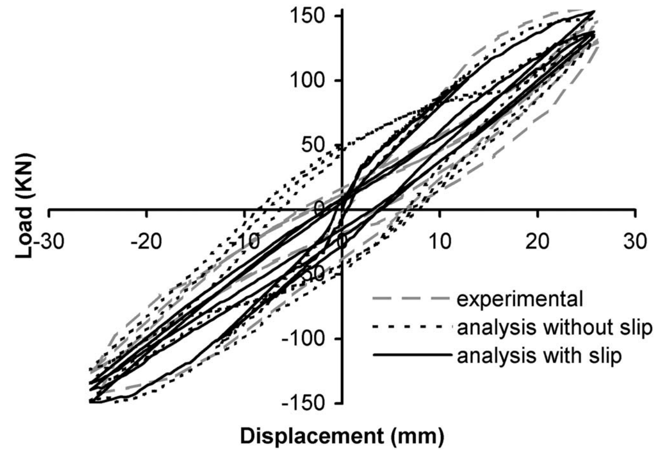

Fig. 11. Comparison of analytical predictions versus experimental measurements for cycles up to ±26 mm

inside the joint (from 90 cm to 150 cm measured from the bottom of the specimen), the bond stress gradually reaches the τ_1 strength (curves A and B) and then it deteriorates to τ_3 (curves C and D) developing a maximum slippage of about 8.5 mm at the bar end.

Interior Beam-Column Joint

The beam-column connection tested by Del Toro Rivera (1988) and analyzed by Fleury et al. (1999), was chosen as a second application. The joint setup intended to simulate the behavior of a connection within a multistory frame during an earthquake (Fig. 10). The uniaxial compressive concrete strength was measured $f_c = 40$ MPa whereas steel yield strength was $f_{s,\Phi 10} = 570$ MPa, $f_{s,\Phi 12} = 490$ MPa, $f_{s,\Phi 14} = 440$ MPa, $f_{s,\Phi 20} = 554$ MPa, and steel initial elastic modulus $E_s = 200$ GPa.

First, a 200 KN compressive force was applied on the columns to simulate the vertical loads of the upper floors. The vertical loads of the considered floor were simulated by imposing a vertical displacement equal to 1.12 mm upon the beam extremities. Finally, a static horizontal cyclic displacement at the column's lower end was applied to simulate the seismic action.

Fifty-six 3D solid elements were used to model the joint, and reinforcement was embedded within the mesh. The applied displacement history of cycles between the values of 13 mm, 26 mm, and 39 mm, as well as the assumed boundary conditions, may be seen in Fig. 10.

The interface for all longitudinal bars inside the core of the connection and for a length equal to two concrete elements around it, was assumed to have a nonlinear behavior. In the remaining lengths, slipping was assumed to be elastic. For simplicity reasons, a unique envelope was chosen to describe the nonlinear bond stress-slip relationship: $\tau_1 = 18$ MPa, $\tau_3 = 3$ MPa, $s_1 = 1$ mm, $s_2 = 3$ mm, $s_3 = 10$ mm. These properties were chosen as intermediate values of the ones used by Fleury et al. (1999) in his 2D discrete finite-element implementation where different values along a bar depending on its position with respect to the core, its stress state (tensile or compressive), its estimated level of confinement and its bond quality (poor or good) had been suggested according to formulas given in Fleury (1996). Especially for τ_1, several values near the average of those derived from this investigation were tested (within a range of ±3 MPa) and 18 MPa was the one giving the most realistic predictions. This bond strength is much larger than the one used for the previous application, since in this example, the confinement of longitudinal bars inside the joint is much higher due to the column axial load.

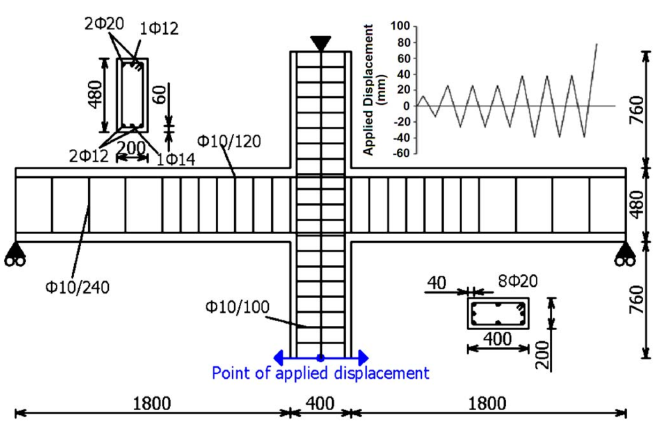

Fig. 10. Experimental test of Del Toro Rivera (1988). All lengths are in mm.

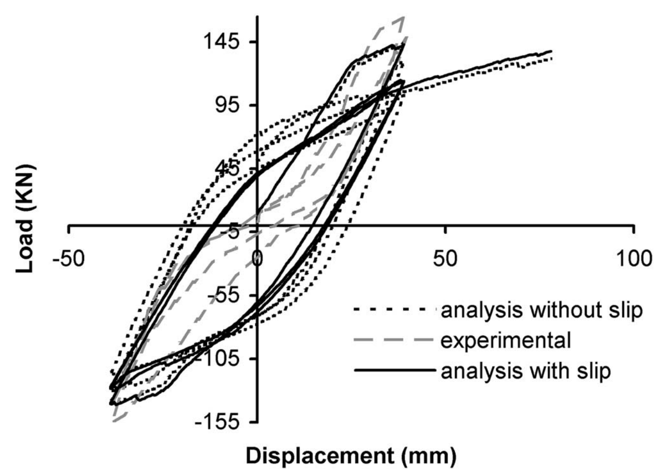

Fig. 12. Comparison of analytical predictions versus experimental measurements only for cycles ±39 mm

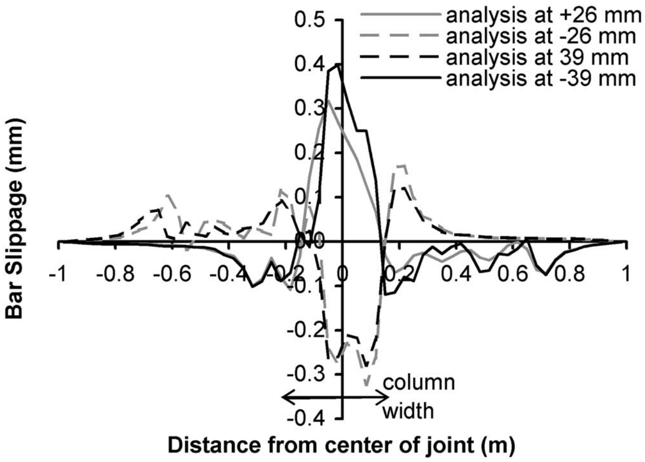

Fig. 13. Bar slippage distribution along beam lower reinforcement bar at ±26 and ±39 mm cycles

The resulting force-displacement curves for cycles are presented in Figs. 11 (cycles ±26 mm) and 12 (cycles ±39 mm). Very good agreement with experimental results may be observed in regard to strength and stiffness up to the intermediate cycles at 26 mm. The analysis allowing slippage especially gives a much better estimation of the dissipated energy and pinching effect.

For the last cycles at 39 mm, where the structure exhibits high nonlinearities, both analyses underestimate the specimen's strength, something which could be due to the limits of the proposed concrete modeling [see also Spiliopoulos and Lykidis (2006)]. Additionally, although the dissipated energy predicted by the analysis allowing slip is smaller than the one predicted by the full bond analysis, curve pinching is much less than the experimental, most probably due to the simplification of using a unique envelope for all points along the bars inside the joint, not reduced by damage.

The slip distribution along the middle lower reinforcement bar inside the beam shows large values in the area inside the joint (Fig. 13). Especially for the cycles at ±13 mm, experimental data on the steel stress distribution are available and they compare well with those of the analysis (Fig. 14).

Throughout the experimental test, both well known mechanisms [as classified, for example, in Leon (1990)] of the diagonal

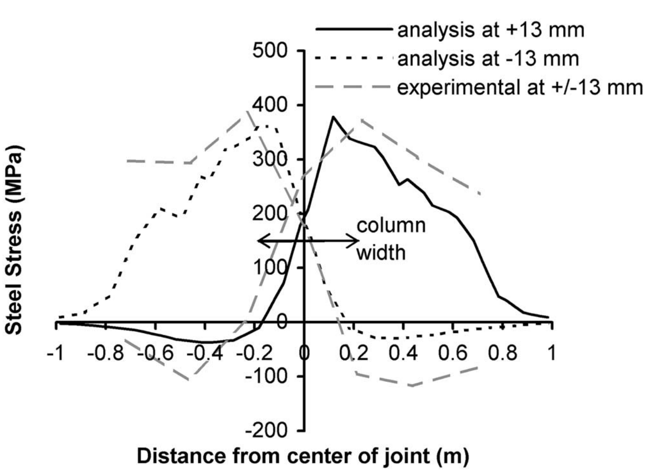

Fig. 14. Steel stress distributions along beam lower reinforcement bar at ±13 mm cycle

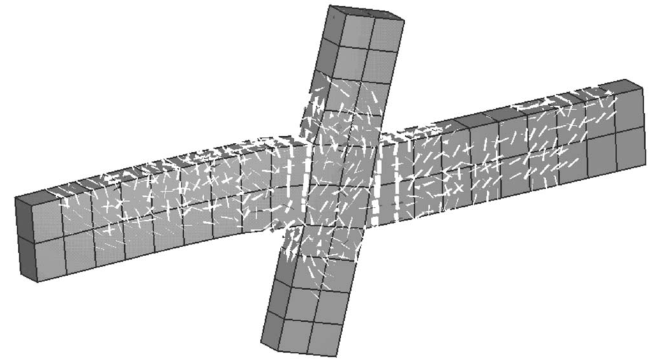

Fig. 15. Predicted cracking at the end of the third cycle of 39 mm

compressive strut (mechanism I) and the panel truss zone (mechanism II) were observed. Initially, in the cycles when steel has not yet yielded and slip levels were low, small diagonal cracks formed inside the joint showing the development of mechanism I. For cycles of larger displacements, when vertical cracks start to extend throughout the beam height due to its flexural reinforcement yielding and slipping together with the formation of a number of smaller diagonal parallel struts throughout the joint, the second mechanism (II) starts to play an important role.

The predicted crack pattern at the end of the cycles at 39 mm is shown in Fig. 15. The characteristics of the second mechanism (II) are well given by the analysis, as shown by the vertical flexural thick cracks at the beam sections near the joint. The diagonal compression resulting from both mechanisms is also indicated by the presence of the diagonal cracks.

In the response predicted for the interior joint, the differences between the analysis with perfect bond and that one with partial bond are less pronounced than those exhibited in the case of the exterior joint. This is the result of the fact that the exterior joint was designed with a limited anchorage length for the longitudinal bars, making it highly bond critical, whereas the interior one was designed according to ACI318-83 for ductile failure.

Conclusions

A relatively simple 3D solid finite-element model has been presented for the analysis of RC structures. The only concrete parameter required is its uniaxial compressive strength. The model refines a previously published work to cater for slippage of reinforcing bars. The embedded reinforcement with slip formulations, together with an interface material model that can give a bond stress prediction for any slip history, seem to bind well in cyclic loading analyses. Despite the many sources of pronounced nonlinearities regarding modeling of crack opening and closure and modeling of the bond-slip behavior, the procedure always gives stable results. It is in favor of the proposed model that although using few elements with simplifying assumptions regarding the bond slip properties, meaningful results may be obtained. The results are in a good agreement with experiments and show that consideration of slippage of the reinforcement is essential to have realistic predictions for analyses of RC joints.

Acknowledgments

Financial support for this work, for the first writer, was provided by the "IRAKLEITOS Basic Research oriented Fellowships," cofunded by the European Social Fund (75%) and National Resources (25%). This support is gratefully acknowledged.

References

ACI Committee. (1997). "Finite element analysis of fracture in concrete structures: State of the art report." *Rep. No. 446:3E-97*, ACI, Detroit.

Ayoub, A. (2006). "Nonlinear analysis of reinforced concrete beam-columns with bond-slip." *J. Struct. Eng.*, 132(11), 1177–1186.

Ayoub, A., and Filippou, F. C. (1999). "Mixed formulation of bond-slip problems under cyclic loads." *J. Struct. Eng.*, 125(6), 661–671.

Barzegar, F., and Maddipudi, S. (1994). "Generating reinforcement in finite-element modelling of concrete structures." *J. Struct. Eng.*, 120(5), 1656–1662.

Barzegar, F., and Maddipudi, S. (1997). "Three-dimensional modelling of concrete structures. II: Reinforced concrete." *J. Struct. Eng.*, 123(10), 1347–1356.

Bathe, K. J. (1996). *Finite element procedures*, Prentice-Hall, Upper Saddle River, N.J.

Bazant, Z. P. (1976). "Instability, ductility and size effect in strain softening concrete." *J. Engrg. Mech. Div.*, 102(2), 331–344.

Bazant, Z. P. (1984). "Imbricate continuum and its variational derivation." *J. Eng. Mech.*, 110(12), 1693–1712.

CEB. (1996). "RC Elements under cyclic loading." *State of the art report*, Thomas Telford, London.

CEB-FIP. (1993). *CEB-FIP model code 1990*, Thomas Telford, London.

Ciampi, V., Eligehausen, R., Bertero, V., and Popov, E. P. (1982). "Analytical model for concrete anchorages of reinforcing bars under generalized excitations." *UCB/EERC No. 82-23*, Earthquake Engineering Research Center, Univ. of California, Berkeley, Berkeley, Calif.

Coronelli, D., and Mulas, M. G. (2001). "Local-global approach in the seismic analysis of R/C frames including bond slip effects." *Eng. Struct.*, 23(8), 911–925.

Del Toro Rivera, R. (1988). "Behavior of reinforced concrete beam-column joints under alternated loading." Ph.D. thesis, Ecole Nationale des Ponts et Chaussées, Paris.

Eligehausen, R., Popov, E. P., and Bertero, V. V. (1983). "Local bond stress-slip relationships of deformed bars under generalized excitations." *UCB/EERC No. 83-23*, Earthquake Engineering Research Center, Univ. of California, Berkeley, Berkeley, Calif.

Elwi, A. E., and Hrudey, T. M. (1989). "Finite element model for curved embedded reinforcement." *J. Eng. Mech.*, 115(4), 740–754.

Fedeas Library. (2006). ⟨http://www.ce.berkeley.edu/~filippou/Research/fedeas.htm⟩ (Apr. 17, 2006).

Filippou, F. C., Popov, E. P., and Bertero, V. V. (1983). "Effects of bond deterioration on hysteretic behaviour of reinforced concrete joints." *UCB/EERC No. 83-19*, Earthquake Engineering Research Center, Univ. of California, Berkeley, Berkeley, Calif.

Fleury, F. (1996). "Prediction of the behaviour of reinforced concrete structures subjected to seismic loading: Proposal of a global model for beam/column joints integrating the behaviour of steel/concrete bond." Ph.D. thesis of Blaise Pascal—Clermond II Univ., France.

Fleury, F., Reynouard, J. M., and Merabet, O. (1999). "Finite element implementation of a steel-concrete bond law for nonlinear analysis of beam-column joints subjected to earthquake type loading." *Struct. Eng. Mech.*, 7(1), 35–52.

Girard, C., and Bastien, J. (2002). "Finite element bond slip model for concrete columns under cyclic loads." *J. Struct. Eng.*, 128(12), 1502–1510.

Hartl, H. (2002). "Development of a continuum mechanics based tool for 3d FEA of RC Structures and application to problems of soil-structure interaction." Ph.D. thesis, Faculty of Civil Engineering, Graz Univ. of Technology.

Jirasek, M., and Bazant, Z. P. (2002). *Inelastic analysis of structures*, Wiley, West Sussex, England.

Kotsovos, M. D., and Pavlovic, M. N. (1995). *Structural concrete, finite element analysis for limit state design*, Thomas Telford, London.

Kwak, H. G., and Filippou, F. C. (1997). "Nonlinear FE analysis of R/C structures under monotonic loads." *Comput. Struct.*, 65, 1–16.

Leon, R. T. (1990). "Shear strength and hysteretic behaviour of interior beam-column joints." *ACI Struct. J.*, 87(1), 3–11.

Limkatanyu, S., and Spacone, E. (2003). "Effects of reinforcement slippage on the nonlinear response under cyclic loadings of RC frame structures." *Earthquake Eng. Struct. Dyn.*, 32, 2407–2424.

Lowes, L. N. (1999). "Finite element modeling of reinforced concrete beam-column bridge connections." Ph.D. thesis, Univ. of California, Berkeley, Berkeley, Calif.

Lowes, L. N., Moehle, J. P., and Govindjee, S. (2004). "Concrete-steel bond model for use in finite element modelling of RC structures." *ACI Struct. J.*, 101, 501–511.

Luiki, M. (1999). "Rahmenecke als netzbewehrte Schubscheibe." MSc thesis, Institute for Structural Concrete, TU-Graz, Graz.

Lykidis, G. C., and Spiliopoulos, K. V. (2006). "A 3d solid finite element for reinforced concrete analysis allowing slippage of reinforcement." *Proc., ECCM 2006* (CD-ROM), Lisbon, Portugal.

Menegotto, M., and Pinto, P. E. (1973). "Method of analysis for cyclically loaded reinforced concrete plane frames including changes in geometry and non elastic behaviour of elements under combined normal force and bending." *Proc., IABSE Symp. on Resistance and Ultimate Deformability of Structures Acted on by Well Defined Repeated Loads*, Lisbon, Portugal, 15–22.

Monti, G., Filippou, F. C., and Spacone, E. (1997). "Finite element for anchored bars under cyclic load reversals." *J. Struct. Eng.*, 123(5), 614–623.

Monti, G., and Spacone, E. (2000). "Reinforced concrete fiber beam element with bond-slip." *J. Struct. Eng.*, 126, 654–661.

Rabczuk, T., Akkermann, J., and Eibl, J. (2005). "A numerical model for reinforced concrete structures." *Int. J. Solids Struct.*, 42, 1327–1354.

Rashid, Y. R. (1968). "Analysis of prestressed concrete pressure vessels." *Nucl. Eng. Des.*, 7(4), 334–344.

Spiliopoulos, K. V., and Lykidis, G. C. (2006). "An efficient three dimensional solid finite element dynamic analysis of reinforced concrete structures." *Earthquake Eng. Struct. Dyn.*, 35, 137–157.

Viwathanatepa, S., Popov, E. P., and Bertero, V. V. (1979). "Effects of generalized loadings on bond in reinforcing bars embedded in confined concrete blocks." *UCB/EERC No. 79-22*, Earthquake Engineering Research Center, Univ. of California, Berkeley, Berkeley, Calif.